ELSEVIER

Chemical Engineering Journal 91 (2003) 249–255

Chemical Engineering Journal

www.elsevier.com/locate/cej

CFD simulation of "gauze pad–honeycomb" catalytic system

Vladimir P. Zakharov, Ilya A. Zolotarskii*, Valerii A. Kuzmin

Siberian Branch of the Russian Academy of Sciences, Boreskov Institute of Catalysis, 5, Akad. Lavrentiev Avenue, 630090 Novosibirsk, Russia

Abstract

The paper is devoted to studies of gas flows and mass transfer in a two-stage catalytic system recently applied in ammonia oxidation at nitric acid plants. Numerical studies are performed by reducing a system to a flat-periodical set of slit channels. Mathematical model based on two-dimensional Navier–Stokes equations with periodicity boundary conditions is used. Dependence of a system performance on a distance between stages is investigated and found to have a non-monotonous character.

Keywords: Ammonia; Nitric acid; Catalyst; Monolith; Numerical model; Gas flow; Pressure drop; Mass transfer; Conversion

1. Introduction

Honeycomb monolith catalysts are widely used for gas phase catalytic reactions [1,2]. Particularly, they have found recently an application as the second catalytic stage in ammonia oxidation reactors in nitric acid plants [3]. In these reactors the conventional platinum-rhodium gauze pad serves as the first catalytic stage. But a number of gauzes in the two-stage system is significantly reduced comparing with a single-stage one [3].

We failed to find any literature data on gas flow and mass transfer in the above-mentioned two-stage system, although each stage is known and has been studied previously. Thus, when there is a considerable distance between the gauze bed and the frontal surface of the structured bed, the stages may be considered independently. However, if the catalyst beds are arranged at a short distance, they may interact dynamically and produce a combined effect on the reaction gas flow and mass-transfer intensity.

So, ad hoc theoretical analysis of the two-stage ammonia oxidation process is needed. We have implemented a study of the problem by the computational fluid dynamics methods. The main object of our work is to clarify how the conversion and other process characteristics depend on the distance between the catalytic stages.

2. Problem statement

Honeycomb channels are square section, rectilinear, co-directional and orthogonal to the gauze pad. Simulation of real three-dimensional processes in a two-stage catalyst system is a rather intricate problem. To simplify the task geometrically, one may reduce it to a single-plate model, which considers the catalytic system as a two-dimensional infinite flat-periodic structure and assumes the channel walls to be impenetrable solid plates of finite thickness. We have studied this two-dimensional problem.

The two-stage catalytic system geometry under the study is illustrated in Fig. 1, which shows one single-plate period. The gas flow at the inlet boundary of the calculation domain is considered as flat-parallel and directed from left to right, but not certainly parallel to the longitudinal axis.

The mathematical model based on two-dimensional Navier–Stokes equations coupled with a mass balance equation for a key reagent is formulated for the above geometrical object in the Appendix A. The mass balance equation accounts for diffusion in both directions. Boundary conditions of periodicity (i.e. equality of function values on upper and lower boundaries), Dirichlet conditions on inlet, zero Neumann outlet conditions and zero-slip conditions on solid walls were used. Closing models are only applicable to the Ω_P domain.

The gas flow is assumed to be viscous, laminar, isothermal, and incompressible (last two assumptions justification is a result of engineering evaluations). The gauze pad is supposed to have isotropic and homogeneous properties. Only heterogeneous reactions are assumed to proceed over both catalyst stages. The catalyst activity is suggested to be

* Corresponding author. Tel.: +7-383-2-34-44-91; fax: +7-383-2-34-18-78.
E-mail addresses: xap@catalysis.nsk.su (V.P. Zakharov), zol@catalysis.nsk.su (I.A. Zolotarskii), kva@catalysis.nsk.su (V.A. Kuzmin).

1385-8947/02/$ – see front matter
PII: S1385-8947(02)00161-4

Nomenclature

C	dimensionless key reagent concentration
d	gauze wire diameter (m)
D_0	diffusion coefficient (m^2/s)
G_0	cell feed flow rate (m^3/s)
h	space-integration step (mm)
H	period of honeycomb monolith structure (mm)
H_0	thickness of honeycomb monolith wall (mm)
j	$(D_0 \partial C/\partial x_2)/V_1^0$, local mass transfer rate on lateral surface of plate
L_P	gauze pad thickness (mm)
P	pressure ($kg/(m\,s^2)$)
$P_{i.a.}$	static pressure at the axis of channels inlet
P_0	reference pressure (atm)
P_∞	pressure drop through gauze pad ($kg/(m\,s^2)$)
Re^0	$\rho_0 V_1^0 H/\mu_0$, intrachannel Reynolds number
Re_ε	$\rho_0(\lvert\vec{V}\rvert/\varepsilon)d/\mu_0$, intrapore Reynolds number
$\Re$	coefficient of gas flow force interaction with porous medium ($kg/(m^3\,s)$)
Sc	$\mu/\rho D_0$, Schmidt number
t	time (s)
T_0	reference temperature (K)
U	V_1/V_1^0, dimensionless longitudinal gas flow velocity component
V_i	longitudinal ($i=1$) and transversal ($i=2$) gas flow velocity components (m/s)
V_1^0	gas flow velocity (m/s)
$\vec{V}$	gas velocity vector
x_i	axial ($i=1$) and transversal ($i=2$) spatial coordinates

Greek letters

β	mass transfer coefficient at the gauze catalyst surface (m/s)
Γ_i	calculation domain boundaries
δ	interstage distance (mm)
ε	gauze pad porosity
η_0	total ammonia conversion over the gauze pad (%)
η_1	total ammonia conversion increment over the frontal surface of plate (%)
η_2	total ammonia conversion increment over the lateral surface of plate (%)
λ	effective length of recirculating flow zone (mm)
μ	molecular viscosity ($kg/(m\,s)$)
π	$((P_0 - P_{i.a.}) - P_\infty)/P_\infty$, dimensionless inlet static pressure drop in channels
ρ	density (kg/m^3)
σ	specific surface area of gauze catalyst (m^{-1})
τ	time-integration step (s)
ψ	stream-function
ψ_-	$\min(\psi/G_0)$, relative intensity of back flow in recirculating flow zone
Ω_0	wall of honeycomb monolith channel
Ω_P	porous medium (gauze pad)

extremely high that imposes the mass transfer limitation and provides zero concentration at a catalyst surface. Gas flow force and chemical interaction within the gauze pad are described in terms of effective porous medium approximation with a closing models for the computation of $\Re$ [4] and β [5].

Resulting numerical solution of the model equations are time dependent two-dimensional fields of gas flow velocity vector, pressure and key reagent concentration.

3. Numerical procedure

An original numerical code was developed for the simulation.

The model equations were solved using primitive physical variables. The equations were approximated on the base of the finite element principle. The velocity components and concentration were represented on piecewise-bilinear basis, pressure on piecewise-constant basis. In the evolutionary algorithm, linearization and decoupling of particular model equations was based on the Rounge–Cutta scheme of second order of accuracy. An implicit Euler scheme was used to approximate the diffusion terms. Discrete diffusion/convection autonomous equations were solved using a version of the ORTHOMIN method [6]. The pressure field was determined by an original unpublished SIMPLE-like procedure (prototype see in [7]). The SLAE scaling [8] was applied to provide the convergence of iteration algorithms.

4. Flow conditions

Calculations were performed using model constants corresponded to the air flow with operation parameters $P_0 = 7$ atm and $T_0 = 900\,^\circ$C, typical for reaction zone in a real catalytic reactor for ammonia oxidation in high-pressure nitric acid plants. Under such conditions $\rho_0 = 2.12\,kg/m^3$ $\mu_0 = 5.04 \times 10^{-5}\,kg/(m\,s)$, $D_0 = 3.66 \times 10^{-5}\,m^2/s$. Gas flow velocity V_1^0 was equal to 4.3 m/s that corresponds to laminar gas flow between plates (i.e. within structured catalyst channels): $Re^0 \approx 1200$.

The model geometry corresponded to those of conventional monoliths and woven gauze pads generally used in Russian nitric acid plants: $L_P = 0.0018\,m$, $d = 10^{-4}\,m$, $\varepsilon = 0.8$, and $\sigma = 10^4\,m^{-1}$. Flat-periodic cell sizing was performed by two different ways. The first is characterized by walls of the same thickness as in honeycomb (*A variant*): $H_0 = 2$ mm. In another one, a structural period has the same value as that in a real monolith (*B variant*): $H = 7$ mm. An open frontal area of a model structure always has the same value as for honeycomb bed, thus $H = 4$ mm in *A variant* and $H_0 = 3.5$ mm in *B variant*. Since the main attention was focused on processes in the vicinity of honeycomb channel inlet, $L_0 = 0.01\,m$ and $L_- = 0$ were set. At varying δ, the L_+ value was set so that $L_+ + \delta = 0.005\,m$.

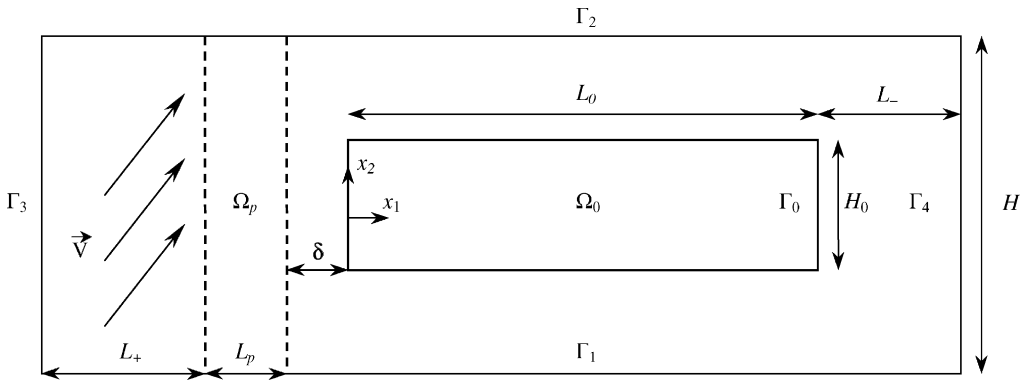

Fig. 1. Calculation domain.

5. Simulation results

Preliminary investigation was devoted to problem of determination of refracting properties of the first oxidation stage. Calculations showed almost absolute refracting properties of the gauze pad with the specified parameters. It means that the porous bed with given properties inhibited the transversal component of the gas velocity so heavily that the gas flows downstream the gauze pad almost in parallel to the monolith channel axis independently on the angle of flow attack. This result proves the validity of our local problem statement and is confirmed analytically.

Therefore, further studies were only reasonable for the case of the longitudinal gas flow upstream the gauze pad. In this case the gas flow is symmetric about the longitudinal axis and the computations were only performed in the upper region of the calculation domain. In this regard, the boundary periodicity conditions were substituted for the symmetry and non-penetration flow conditions.

The computations were performed using quite fine computational grid with an equal-sized spatial step $h = 1/40$ mm. In such a way, the number of nodes finally was 669×141 for *B variant* and total number of unknown variables including two velocity vectors and pressure and concentration field vectors reached about 260 000.

Since non-stationary pulsating regimes were detected, time-averaging of numerical solutions was realized. A time-integration step was adjusted equal to 1×10^{-5} s. The decision to terminate the averaging was adopted based on visual inspection of the averaged flow and concentration fields, as well as on the control of such numerical characteristics as the rate of the fields' change and the stability of integral mass transfer. To accomplish a computation procedure, 10^5 time steps were needed sometimes.

5.1. Gas flow structure

The gas flow structures were first studied. Some qualitative results are exemplified in Figs. 2 and 3.

It was discovered that when both stages touch with each other, gas flow is stationary and free of any recirculating flow zones (Fig. 3a). When the gap between stages δ is a small non-zero value, gas flow keeps the property of stability but small and low-intensive clockwise recirculating flow zone appears just behind the edge of the channel inlet. As the gap is further widened, the gas flow mode becomes unsteady pulsating and a sequence of separated vortexes is generated from the recirculating flow zone (Fig. 2). The separated vortexes move downstream and dissipate. At the same time the effective recirculating flow zone lengthens

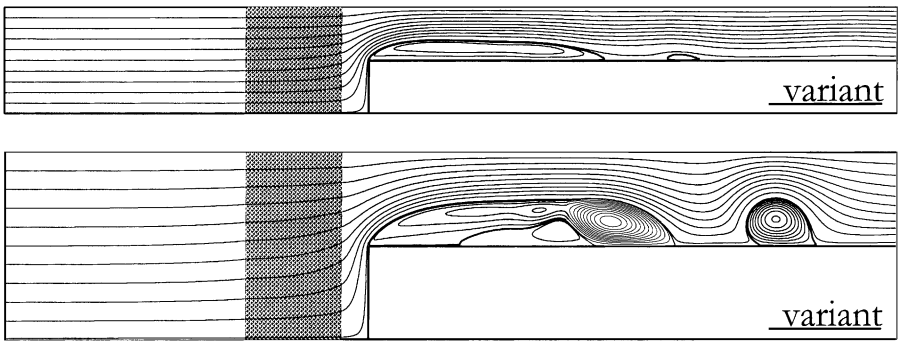

Fig. 2. Momentary streamlines: $\delta = 0.5$ mm. Contour interval for dimensionless streamfunctions is $\Delta\psi = 0.1$ for basic stream and $\Delta\psi = 0.02$ for recirculating stream. Streams separating line is drawn thickly.

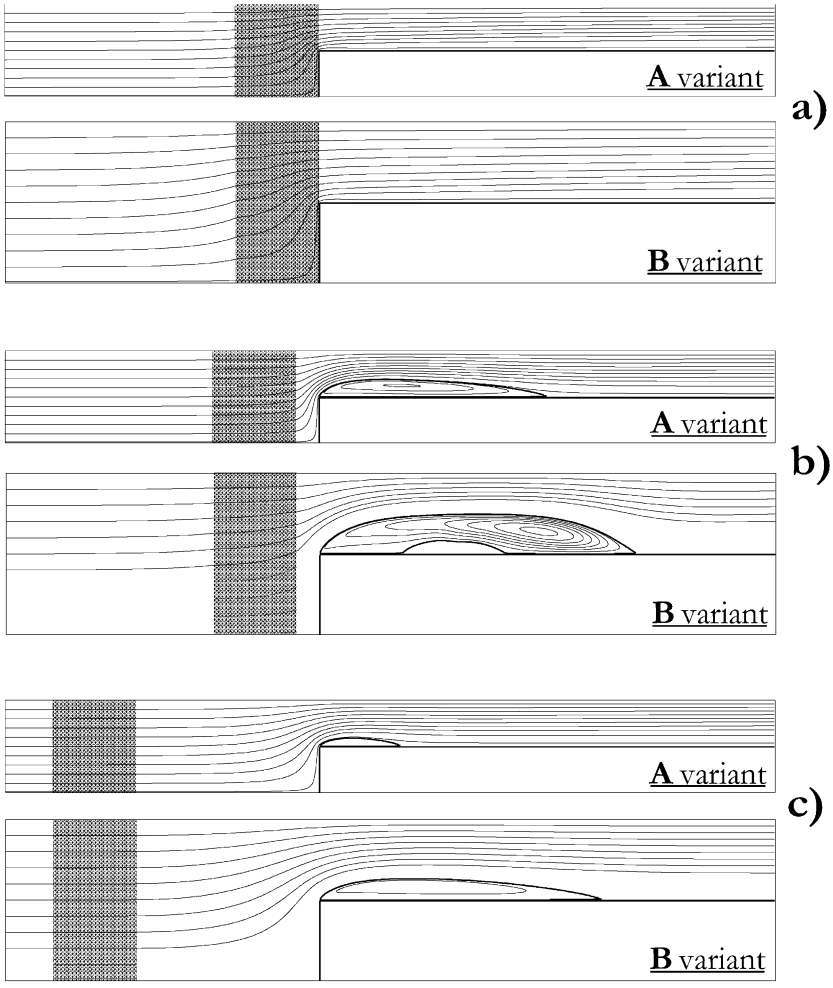

Fig. 3. Time-averaged streamlines: (a) $\delta = 0$ mm; (b) $\delta = 0.5$ mm; (c) $\delta = 4.0$ mm. Contour intervals correspond to ones in Fig. 2.

(Fig. 3b) although remains comparatively short against the length of the vortexes existence region. When the distance between stages δ increases, the flow keeps the pulsation nature, while its instability diminishes, intensity of vortexes generation relaxes, and the effective size of the recirculating flow zone decreases to a non-zero value (Fig. 3c). Consequently, numerical results show that the nature of flow about honeycomb wall changes in non-monotonous manner with increasing δ. An interesting distinctive feature of the flow under study is the presence of tertiary counter-clockwise vortex within secondary clockwise separated convection zone (see Fig. 3b).

5.2. Gas flow characterization

Velocity distributions through channel inlet are represented in Fig. 4. It is important, that they are very multiform: the "inverted" profiles (i.e. one with an apparent maximum nearby the channel wall) of longitudinal velocity at $\delta \approx 0$ (Fig. 4a and b; scale unit is V_1^0) but almost uniform profiles at $\delta \geq H_0$ (Fig. 4e) are observed.

Fig. 5a illustrates the effective length of recirculating flow zones. The plot in Fig. 5b shows the effective intensity of recirculating flows in these zones defined as a relative amount of gas moving there from right to left. In other words, these are dependencies of extremal negative values of dimensionless streamfunctions (scale unit is G_0). It is interesting that

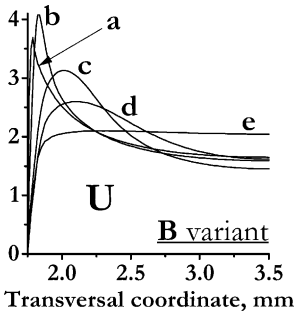

Fig. 4. Time-averaged dimensionless longitudinal velocity profiles on channels inlet: (a) $\delta = 0$ mm; (b) $\delta = 0.1$ mm; (c) $\delta = 0.5$ mm; (d) $\delta = 1.0$ mm; (e) $\delta = 4.0$ mm.

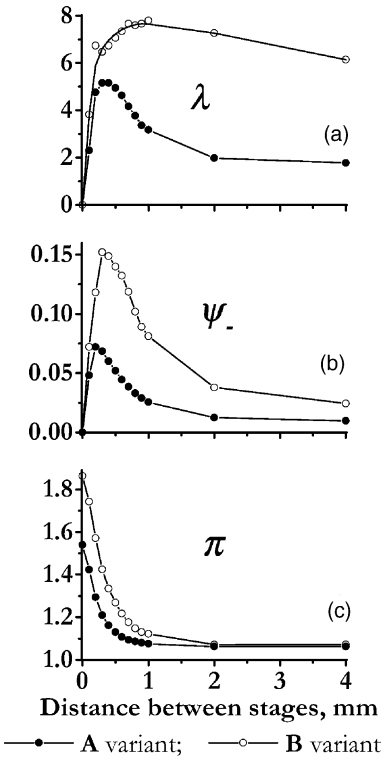

Fig. 5. Time-averaged gas flow characteristics: (a) effective length of recirculating flow zones; (b) effective intensity of recirculating flows; (c) inlet pressure drop.

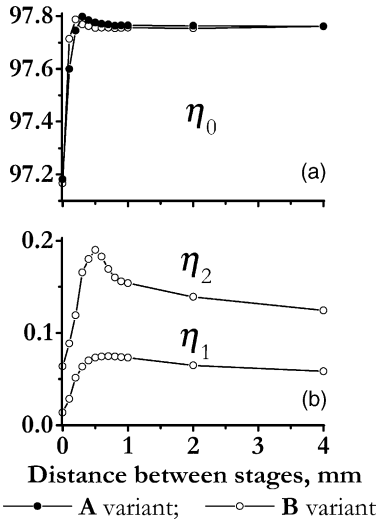

Fig. 6. Time-averaged total mass transfer characteristics: (a) total conversion over the gauze pad; (b) portion of conversion over the plate surfaces.

instantaneous convection intensity in each single vortex is several times higher than that in the time-averaged stream.

From analysis of pressure distribution within the channels, pad-to-monolith distance δ effects essentially the pressure drop at the channel inlet (Fig. 5c; scale unit is $P_\infty \approx -940\,\mathrm{kg/(m\,s^2)}$). At a small gap, there is a very significant inlet pressure drop but, as δ increases, decreases quickly from large values to P_∞. This kind of dependence can influence gas flow velocity distribution on the macro scale of the whole reactor dramatically and must be taken into consideration when designing two-stage catalytic systems. Notice that experimental pressure drop values measured with real monoliths and gauze pads for the cases of zero- and non-zero inter-stage distances at the bench scale are not so different as the calculation show but by ≈20% only (Vostrikov, private communication).

5.3. Mass transfer

5.3.1. Mesh reactor

The total conversion over the gauze pad was found to be almost monotonic and strongly dependent on the distance between catalyst beds when this distance is small (Fig. 6a). The minimum conversion corresponds to zero distance. This effect is accounted for by the character of power dependence of β on Re_ε (exponent is less then 1, i.e. the dependence is convex upwards). Thus, the mass transfer intensity decrease nearby the plate frontal surface, where the gas velocity is low, is not compensated by its increase a little way away, where the gas velocity is comparatively high. Feebly marked local maximums could be attributed to penetration of non-stationary stream perturbations into the bulk of the gauze pad, that intensifies the process. Interestingly, the reagent diffusion along the flow causes a considerable (1–3%) decrease in the reagent concentration at the upstream side of gauze catalyst bed Ω_P.

5.3.2. Monolith reactor

As regards time-averaged mass transfer intensity at the entrance region of the second oxidation stage channel on distance δ, it is strongly non-monotonous for the lateral plate surface and slightly non-monotonous for the frontal one (Fig. 6b). These effects culminate at $\delta \approx 0.5$ mm, when vorticity is maximal. Minimum values are attained at $\delta = 0$, when the flow is steady-state and the plate is flowed about by a very depleted stream. The depletion concentration layer along the lateral plate surface lasts for a quite long distance because of the above-mentioned inlet longitudinal velocity profile (Fig. 4a). At $\delta > 0.5$ mm mass transfer rate at the channel inlet comes down because of subsiding flow fluctuations.

Local mass transfer rate (j) distributions along the lateral plate surface are extremely non-monotonous (Fig. 7). They have minimums at recirculating flow zones and maximums—at reattaching flow ones. Values of these extremums have an extremal dependence on δ as well. This happens due to described above flow structure evolutions. At large δ asymptotic dependence is reached. It is shaped in qualitative coincidence with mass transfer measurements performed by Hwang et al. [9] for a turbulent regime and contradict significantly to recognized [10,11] or more novel [12–14] monotonic correlations. All these correlations are applicable for a gas flow about a plate with a zero thickness.

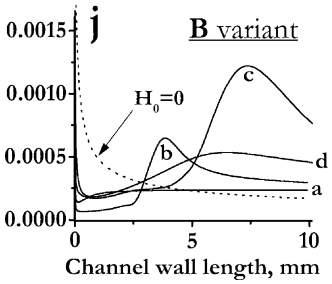

Fig. 7. Time-averaged local mass transfer rate: (a) $\delta = 0$ mm; (b) $\delta = 0.1$ mm; (c) $\delta = 0.5$ mm; (d) $\delta = 4$ mm.

We have performed computations for the case of zero wall thickness to demonstrate the importance of influence of channel wall thickness on the mass transfer process at the honeycomb channel. The calculated curve is plotted with dotted line in Fig. 7. One can see that mass transfer in a real honeycomb is very different from what is commonly used in correlations even when a distance between stages is large enough.

6. Conclusion

The two-dimensional model is developed for the numerical calculation of the non-steady-state laminar-vortex mass transfer in the flat-periodic channels system. Mathematical modeling of ammonia oxidation on a two-stage catalytic system corresponding to high pressure nitric acid plant was performed. The regularities obtained characterize variations in local and total mass transfer rates both on frontal and lateral surfaces of the channel walls and within the gauze pad. Non-steady vortex generation is shown to have the important role in mass transfer processes.

The main results of the study are the following:

- Channel stream structure has a remarkably non-monotonous dependence on a distance between two catalytic stages. There may be either steady-state non-separated convection or pulsating one with recirculating flow zones. A system pressure drop sharply increases with a close approaching of the stages.
- An optimal distance exists with regard to ammonia conversion both in a whole system and in each stage.
- Local mass transfer rate in a honeycomb channel is shown to have a complex spatial dependence with maximum and minimum which differs fundamentally from commonly used correlations do not account for nature of gas flow about a channel wall.

The presented study stimulates further investigations to obtain reliable mass transfer correlations for real flow conditions at the entrance region of honeycomb channels. Results of these studies are fundamentally important not for reaction conversion only but especially for complex reactions where a selectivity is of particular interest.

Appendix A. Mathematical model formulation

Momentum equations:

$$\rho_0\left[\frac{\partial V_1}{\partial t} + V_1\frac{\partial V_1}{\partial x_1} + V_2\frac{\partial V_1}{\partial x_2}\right] = \frac{\partial}{\partial x_1}\left(-P + \mu_0\frac{\partial V_1}{\partial x_1}\right) + \frac{\partial}{\partial x_2}\left(\mu_0\frac{\partial V_1}{\partial x_2}\right) - \Re V_1,$$

$$\rho_0\left[\frac{\partial V_2}{\partial t} + V_1\frac{\partial V_2}{\partial x_1} + V_2\frac{\partial V_2}{\partial x_2}\right] = \frac{\partial}{\partial x_1}\left(\mu_0\frac{\partial V_2}{\partial x_1}\right) + \frac{\partial}{\partial x_2}\left(-P + \mu_0\frac{\partial V_2}{\partial x_2}\right) - \Re V_2$$

Continuity equation:

$$\frac{\partial}{\partial x_1}(\rho_0 V_1) + \frac{\partial}{\partial x_2}(\rho_0 V_2) = 0$$

Mass transport equation:

$$\frac{\partial C}{\partial t} + V_1\frac{\partial C}{\partial x_1} + V_2\frac{\partial C}{\partial x_2} = \frac{\partial}{\partial x_1}\left(D_0\frac{\partial C}{\partial x_1}\right) + \frac{\partial}{\partial x_2}\left(D_0\frac{\partial C}{\partial x_2}\right) - \sigma\beta C$$

Boundary conditions:

$$V_1|_{\Gamma_1} = V_1|_{\Gamma_2}, \quad V_1|_{\Gamma_3} = V_1^0, \quad \left.\frac{\partial V_1}{\partial x_1}\right|_{\Gamma_4} = 0,$$

$$V_1|_{\Gamma_0} = 0, \quad V_2|_{\Gamma_1} = V_2|_{\Gamma_2}, \quad V_2|_{\Gamma_3} = V_2^0,$$

$$V_2|_{\Gamma_4} = 0, \quad V_2|_{\Gamma_0} = 0, \quad C|_{\Gamma_1} = C|_{\Gamma_2},$$

$$C|_{\Gamma_3} = 1, \quad \left.\frac{\partial C}{\partial x_1}\right|_{\Gamma_4} = 0, \quad C|_{\Gamma_0} = 0$$

Closing models [4,5]:

$$\Re = \frac{1}{d}\left(\frac{1-\varepsilon}{\varepsilon^3}\right)\left[150\mu_0\frac{1-\varepsilon}{d} + 1.75\rho_0|\vec{V}|\right],$$

$$\beta = \frac{D_0}{d}0.395Re_\varepsilon^{0.64}Sc^{0.33}$$

References

[1] A. Cybulski, J.A. Mouljin (Eds.), Structured Catalyst and Reactors, Marcel Dekker, New York, 1998.
[2] R.M. Heck, S. Gulati, R.G. Farrauto, The application of monoliths for gas phase catalytic reactions, Chem. Eng. J. 82 (2001) 149–156.
[3] V.A. Sadykov, L.A. Isupova, I.A. Zolotarskii, L.N. Bobrova, A.S. Noskov, V.N. Parmon, E.A. Brushtein, T.V. Telyatnikova, V.I. Chernyshev, V.V. Lunin, Oxide catalysts for ammonia oxidation in nitric acid production: properties and perspectives, Appl. Catal. A: Gen. 204 (1) (2000) 59–87.
[4] S. Ergun, Fluid flow through packed columns, Chem. Eng. Progr. 2 (1952) 89–94.
[5] M.E. Aerov, O.M. Todes, D.A. Narinskii, Fixed Bed Apparatus, Hydraulic and Thermal Basis of Operation, USSR, Leningrad, Khimiya, 1979.
[6] L.A. Hageman, D.M. Young, Applied Iterative Methods, Academic Press, New York, 1981.

[7] S.V. Patankar, Numerical Heat Transfer and Fluid Flow, Hemisphere, Washington, DC, 1980.
[8] G.E. Forsythe, C.B. Moler, Computer Solution of Linear Algebraic Systems, Prentice-Hall, Englewood Clifs, NJ, 1967.
[9] K.S. Hwang, H.J. Sung, J.M. Hyun, Mass transfer measurements from a blunt-faced plate in an uniform flow, Int. J. Heat Fluid Flow 17 (2) (1996) 179–182.
[10] H. Schlichting, Grenzschicht-theorie, Karlsruhe, 1951.
[11] R.D. Hawthorn, AIChE Symp. Ser. 70 (1974) 428.
[12] V. Grigull, H. Tratz, Int. J. Heat Mass Trans. 8 (1995) 969.
[13] G. Groppi, A. Belloli, E. Tronconi, P. Forzatti, Comparison of lumped and distributed models of monolith catalyst in hybrid combustors for gas turbines, Chem. Eng. Sci. 50 (1995) 2705–2715.
[14] R.E. Hayes, S.T. Kolaczkowski, A study of Nusselt and Sherwood numbers in a monolith reactor, Catal. Today 47 (1999) 295–303.